Int J Clin Exp Med 2025;18(8):208-219
www.ijcem.com /ISSN:1940-5901/IJCEM0164604

Original Article

Isosinensetin attenuates the growth of colorectal cancer cells by targeting the USP10/c-Myc signaling pathway

Ying-Lei Wu, Xiu-Rong Yang, Yao-Hui Yuan

Xingtai Central Hospital, No. 108 Gangtiebei Road, Xindu District, Xingtai 054000, Hebei, China

Received March 18, 2025; Accepted July 8, 2025; Epub August 15, 2025; Published August 30, 2025

Abstract: Objectives: To investigate the effects of Isosinensetin (ISNT) on colorectal cancer (CRC) progression and explore its potential molecular mechanisms. Methods: Cell proliferation was evaluated using the MTT assay; colony formation ability was assessed via plate clone formation assays; Transwell migration and invasion assays were used to determine cell migration and invasion capacity. Cancer cell stemness was analyzed by a tumor spheroid formation assay. Subcutaneous tumor-bearing mouse experiments were performed to observe tumor growth in vivo. Real-time fluorescence quantitative PCR (qPCR) and Western blot analyses were used to examine gene and protein expression. Pull-down assays, luciferase reporter assays, and ubiquitination assays were employed to study protein interactions and degradation pathways. Results: ISNT significantly inhibited the proliferation, migration, invasion, and stemness of CRC cells in vitro. In the mouse tumor model, ISNT suppressed tumor growth. Mechanistically, ISNT reduced the transcriptional activity of ubiquitin-specific peptidase 10 (USP10), thereby promoting USP10-catalyzed ubiquitination and subsequent degradation of the MYC proto-oncogene (c-Myc). Conclusions: ISNT effectively inhibits CRC progression by suppressing cell proliferation, migration, invasion, and stemness. The underlying mechanism involves downregulation of USP10 transcriptional activity, leading to c-Myc ubiquitination and degradation.

Keywords: Isosinensetin, colorectal cancer, USP10, c-Myc

Introduction

Worldwide, colorectal cancer (CRC) accounts for approximately 10% of all cancer diagnoses and cancer-related deaths, ranking second in global cancer mortality and third in incidence [1]. Projections indicate that by 2035, 2.5 million new CRC cases will be reported globally [2]. Despite advancements in CRC therapies, unmet clinical needs persist [3], underscoring the critical importance of developing new, safe, and effective drug molecules for adjunctive CRC treatment.

Ubiquitin-specific peptidase 10 (USP10) mediates diverse physiological and metabolic functions. It deubiquitinates and stabilizes p53 in response to DNA damage [4], activates AMP-activated protein kinase alpha 1 (AMPK) during energy deficiency [5], enhances autophagy by stabilizing Beclin1 [6], and maintains the stability of the notch receptor 1 intracellular domain (NICD1) in endothelial cell angiogenesis [7]. USP10's role in cancer is context-dependent: it acts as a tumor suppressor in gastric [8] and intestinal adenocarcinomas [9], yet promotes oncogenic activity in prostate, breast, and acute myeloid leukemia [10]. However, its specific involvement in CRC remains poorly understood.

Screening drug molecules from natural products is a modern strategy in drug development [11, 12]. For example, dimethyl fumarate (DMF), derived from the methyl ester of natural fumaric acid (a tricarboxylic acid cycle intermediate), and SFX01, developed from natural sulforaphane, are under clinical evaluation for various diseases. Pentacyclic triterpenoids like bardoxolone methyl (RTA 402) and omaveloxolone (RTA 408) are in clinical trials for chronic kidney disease, type 2 diabetes, and pulmonary arterial hypertension [11, 12]. Polymethoxyflavones (PMFs), abundant in citrus species, exhibit diverse pharmacological activities, including anti-tumor [13], anti-inflammatory, [14] antimutagenic [15], antiviral [16], antioxidant [17], and antihypertensive effects [18]. Isosinensetin

https://doi.org/10.62347/SSIF8218

(ISNT), a PMF, has been studied for its anti-tumor, anti-fibrotic, antioxidant, and anti-diabetic properties [17, 19, 20]. However, its impact on CRC and regulation of the USP10/c-Myc signaling pathway remain underexplored.

This study aims to investigate the anti-tumor effects of ISNT in CRC cells and a mouse subcutaneous xenograft model, and to elucidate its interaction with the USP10/c-Myc signaling pathway. These efforts seek to provide experimental and theoretical support for ISNT's potential clinical application in CRC therapy.

Materials and methods

All experimental procedures adhered strictly to the ARRIVE guidelines and were performed in compliance with relevant regulations.

Cells

The human colorectal cancer (CRC) cell lines HCT 116 (CL-0096), RKO (CL-0196) and SW620 (CL-0225) were kindly provided by Wuhan Pricella Biotechnology Co.,Ltd. Cells were cultured respectively in McCoy's 5A, MEM and Leibovitz's L-15 media, with 10% fetal bovine serum from Israel BioIndustries (BI) and 1% penicillin-streptomycin solution (PS, 100×) added to the media. The media were supplied by Muellerunbio in Dalian, China. The cultures were kept in a humidified 5% CO_2 environment during incubation at 37°C. Experiments were carried out after the mycoplasma test was negative.

3-(4, 5-dimethylthiazol-2-yl)-2, 5-diphenyl-2H-tetrazolium bromide (MTT) assay

In order to conduct the experiment, 2.0×10^3 cells of HCT116 cell line and 3.0×10^3 cells of RKO/SW620 cell lines were added to each well of a 96-well plate in a volume of 100 μL. Various concentrations of Isosinensetin (ISNT, the highest concentration was 50 μm, which was successively diluted by 2-fold gradient) were administered twenty-four hours after planting. After the treatment for 72 hours, 10 μL of MTT solution (5 mg/mL, MCE, HY-15924) was applied to every well. Dimethyl sulfoxide (DMSO, 100 μL) was used to dissolve the formazan crystals after four hours of incubation, after which the liquid above the crystals was discarded. Thermo Fisher Scientific's Multiskan FC microplate reader was used to measure the absorbance at 490 nm.

Colony formation assay

1,000 cells of HCT116, RKO or SW620 were added to each well of a 6-well plate. The medium was changed every 3 days and the final concentration of ISNT was 0, 10, 20 and 40 μm. In order to fix the cells, the cells were washed twice with phosphate-buffered saline (PBS) after 14 days and then exposed to 4% paraformaldehyde for 15 minutes. After staining the colonies with 0.1% crystal violet for 15 minutes, photographs were taken.

Cell migration and invasion

Transwell plates with 24-wells were used to evaluate migration and invasion. The upper surfaces of the transwell insert porous membranes were either coated with Matrigel (BD Bioscience) or left uncoated. About 200 μL of serum-free medium mixed with 0, 10, 20 and 40 μm ISNT respectively and 5×10^4 HCT116, RKO or SW620 cells were placed in the upper chambers. The lower wells were filled with 0.5 mL of medium containing 20% FBS as a chemoattractant. Following a 24-hour incubation period, the cells that did not migrate to the upper side of the membrane were carefully eliminated. Afterwards, a 0.1% crystal violet solution from Amresco was used to fix and stain the remaining cells on the lower side.

Quantitative PCR (qPCR)

RNA was extracted from HCT116 and RKO cells using Trizol Reagent (Yeasen, China) and converted into cDNA using Hifair®III 1st Strand cDNA Synthesis Kit. An experiment utilizing 2×SYBR Green Premix PCR Master Mix (Bimake, USA) was performed using a LightCycler®480 (Roche, Switzerland) equipment for real-time PCR. The $2^{-\Delta\Delta Ct}$ technique was used to calculate the expression levels of the target genes, which were normalized to GAPDH. The primer sequence is listed in **Table 1**.

Western blotting

After protein concentration was determined using the Bicinchoninic Acid Assay (BCA) detection kits (Beyotime, China), equal amounts of protein lysates were resolved on 10% sodium

Table 1. Human qPCR primer pairs

Gene	Forward	Reverse
GAPDH	GTTTCTATAAATTGAGCCCGCAG	CGACCAAATCCGTTGACTCC
c-Myc	CCTGGTGCTCCATGAGGAGAC	CAGACTCTGACCTTTTGCCAGG
USP10	AAATGCCACCGAACCTATCGGC	CAGCCATTCAGACCGATCTGGA

dodecyl sulfate polyacrylamide gel electrophoresis (SDS-PAGE) gels and transferred to PVDF membranes. After blocking the membranes with 5% skim milk powder, the membranes were incubated with primary antibodies including anti-c-Myc (Cell Signaling, #5605), anti-USP10 (Proteintech, 67917-1-Ig), anti-Ubiquitin (Cell Signaling, #3936), anti-CD44 (Proteintech, 15675-1-AP), anti-CD133 (Cell Signaling, #64326), anti-OCT4 (Abcam, ab19857), anti-Nanog (Abcam, ab109250) and anti-β-actin (Proteintech, 66009-1-Ig, used as a control) at 4°C overnight. Then, they were incubated with a secondary antibody (1:8000, KPL, 5220-0336) at room temperature for 2 hours. Detection of protein bands was performed using a chemiluminescent WB luminol reagent provided by Santa Cruz Biotechnology, USA.

Sphere-formation assay

The development of tumor spheres was examined by seeding HCT116, RKO and SW620 cells into 96-well ultralow attachment plates (Corning) at a density of 500 cells per well. For this reason, a specific tumorsphere medium was utilized, which contained 20 ng/mL of epidermal growth factor, 10 ng/mL of basic fibroblast growth factor, 5 μg/mL of insulin, 0.4% bovine serum albumin, and DMEM/F12. After 3 days, the tumorspheres that had formed were subjected to different concentrations of ISNT (10, 20 and 40 μm) for another 72 hours. Changes in the morphology and number of spheres were meticulously documented.

Mouse xenograft models

Female athymic nude mice (BALB/c, Charles River; aged six to eight weeks) were purchased from Academy of Military Medical Sciences, (Beijing, China) and housed in sterile isolator cages in a SPF BSL-2 facility. The environment was maintained at 24±1°C, 50±10% humidity, and a 12-h light cycle. Mice received autoclaved food, water, and bedding, with cages changed three times weekly. All animal experiments were performed in accordance with the guidelines of the Institutional Animal Care and Use Committee (IACUC) of Xingtai Central Hospital (Approval number: XTZXYY-SYDWLL-2023-1221).

The mice were utilized for the subcutaneous injection of 5×10^6 HCT116 cells. When the tumor reached 80 to 100 mm^3, the animals were randomly divided into three groups of five mice each. Intraperitoneal injection of ISNT at 100 and 200 mg/kg was performed every day, while control group was injected with distilled water. Measurements of tumor dimensions were taken every three days using a vernier caliper, and the volumes of the tumors were estimated using the equation $V=1/2 \times \text{length} \times \text{width}^2$. The weight of the mice was weighed and recorded every day. After 16 days, the mice were humanely euthanized by CO_2 inhalation, and the tumors were carefully removed and documented through photography.

Hematoxylin and Eosin (H&E) stain

The tissues were fixed with paraformaldehyde, embedded in paraffin, and sectioned into 5 μm slices. The slices were dewaxed in xylene and hydrated in 100%, 95%, 85%, and 75% ethanol for 5 minutes each. After being washed twice with PBS, the slices underwent hematoxylin and eosin staining (Beyotime). Subsequently, the slices were cleared through 75%, 85%, 95%, and 100% alcohol and xylene, air-dried, and mounted with neutral resin.

Pull-down assay

In order to prepare the HCT116 cell lysates for the assay, a lysis solution (20 mM Tris-HCl -pH 7.4, 150 mM NaCl, 10% glycerol, 0.5% NP-40, and 1X NaF) was mixed with 1X cocktail (Yeasen) and PMSF (Solarbio) protease inhibitors. The supernatant was left to incubate with 2 μg of c-Myc antibody overnight at 4°C after centrifugation at 12,000 rpm for 15 minutes. After that, the lysate and antibody combination

were incubated for 2 hours before pre-washed magnetic beads were added. A buffer containing 20 mM Tris-HCl (pH 7.4), 150 mM NaCl, 10% glycerol, and 0.1% Triton X-100 was used to wash the beads many times after incubation. Afterwards, the beads were mixed with SDS-PAGE sample loading buffer (2X), subjected to a 10-minute heating cycle at 95°C, and finally, the mixture was spun at 12,000 rpm for an additional 10-minutes period in order to collect the supernatant for SDS-PAGE examination. The target proteins were located using Liquid Chromatography Tandem-mass Spectrometry (LC-MS/MS, Fusion). The statistical data are shown as the mean plus or minus the standard deviation, and the significance levels are ***P<0.001, **P<0.01, *P<0.05 (Student's t-test).

Statistical analysis

A completely randomized design was adopted, and the cells were divided into 4 groups: the control group (DMSO), the low-dose Isosinensetin group (10 μM), the medium-dose group (20 μM), and the high-dose group (40 μM), with n=3 in each group (the experiment was independently repeated 3 times). All data were recorded as mean ± SD. Student's t-test was used for comparison between groups. The control group was normalized and the percentage of the experimental group to the control group was calculated. In the animal experiment, mice were randomly divided into 3 groups, with 5 mice in each group for the experiment. The data were processed as the mean ± SD, and the components were tested by t-test. Differences were considered significant when the *p* value was less than 0.05. (*P<0.05, **P<0.01, ***P<0.001). The SPSS 18.0 and GraphPad Prism 19.5.1 were used to perform statistical analysis.

Results

ISNT inhibits CRC cell growth in vitro

Isosinensetin (ISNT), a polymethoxyflavone found in various citrus species, exhibits potent anti-tumor activity. As shown in **Figure 1A**, its chemical structure was characterized. Following treatment with increasing doses of ISNT for 72 hours, HCT116, RKO, and SW620 cell growth was significantly inhibited in a dose-dependent manner, with IC_{50} values of 12.76 μM, 14.06 μM, and 14.27 μM, respectively (**Figure 1B**). Microscopic analysis revealed marked morphological alterations in cells treated with 10, 20, and 40 μM ISNT compared to the control group (**Figure 1C**). Colony formation assays further confirmed that these concentrations of ISNT suppressed cell proliferation (**Figure 1D**). Collectively, these results demonstrate that ISNT potently inhibits CRC cell growth in vitro.

ISNT impairs CRC cell migration and invasion in vitro

To assess the impact of ISNT on CRC cell motility, transwell assays with and without Matrigel were performed using HCT116, RKO, and SW620 cells. Results showed a dose-dependent reduction in migration capacity compared to untreated controls (**Figure 2A-D**). Invasion assays similarly revealed that 10, 20, and 40 μM ISNT significantly attenuated cell invasive potential (**Figure 2E-H**). These findings indicate that ISNT suppresses both migration and invasion of CRC cells.

ISNT reduces CRC cell stemness in vitro

Growing evidence highlights the role of cancer stem cell (CSC) stemness in CRC recurrence, metastasis, drug resistance, and poor prognosis [21, 22]. To investigate ISNT's effect on CSC properties, tumor sphere formation assays were conducted. Treatment with 10, 20, and 40 μM ISNT disrupted tumor sphere formation and reduced sphere numbers in a dose-dependent manner across HCT116 (**Figure 3A**), RKO (**Figure 3B**), and SW620 (**Figure 3C**) cell lines (**Figure 3D**). Western blot analysis confirmed that ISNT downregulated expression of CSC biomarkers (**Figure 3E**, **3F**). These results suggest that ISNT diminishes CRC cell stemness.

ISNT suppresses CRC tumor growth in vivo

A subcutaneous tumor xenograft model in nude mice was used to evaluate ISNT's anti-tumor efficacy in vivo. HCT116 cells were inoculated subcutaneously into 6-8-week-old nude mice, and once tumors reached 80-100 mm^3, mice were randomized into three groups: vehicle control, 100 mg/kg ISNT, or 200 mg/kg ISNT (intraperitoneal injection daily). Tumor dimensions were measured every 3 days. After 16 days, mice were euthanized, and tumors were excised for weight and imaging analysis. Body

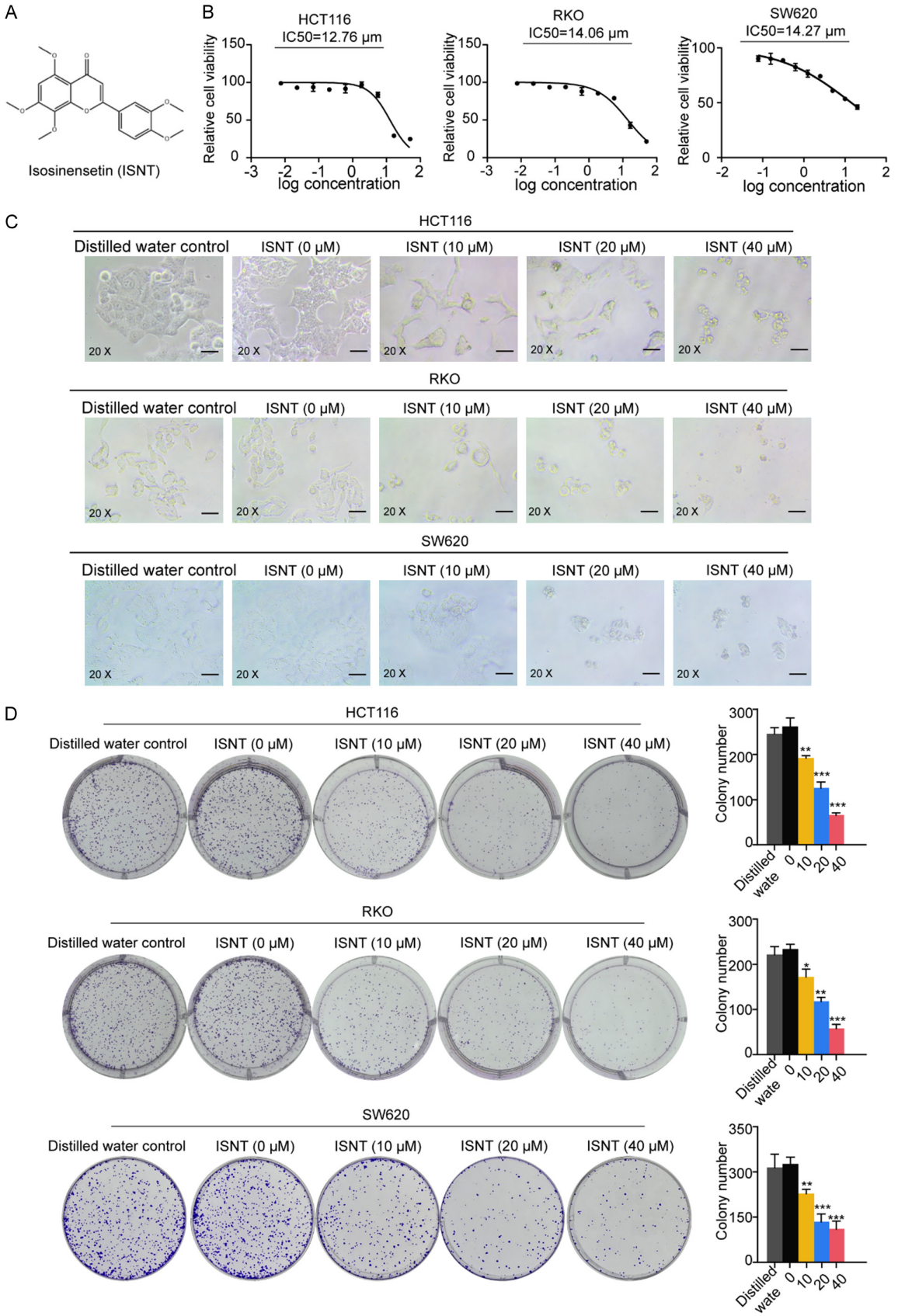

Figure 1. ISNT inhibits the growth of CRC cells in vitro. A: Chemical structure of ISNT. B: The IC_{50} values for HCT116, RKO and SW620 cells were measured after 72 hours of treatment with different doses of ISNT. C: Photos showing

HCT116, RKO and SW620 cells treated with different doses of ISNT for 72 hours. Scale bars represent 100 μm. D: Analysis of colony formation in cells treated with varying concentrations of ISNT. Compared with the control group (ISNT of 0 μm), ***P<0.001, **P<0.01, *P<0.05.

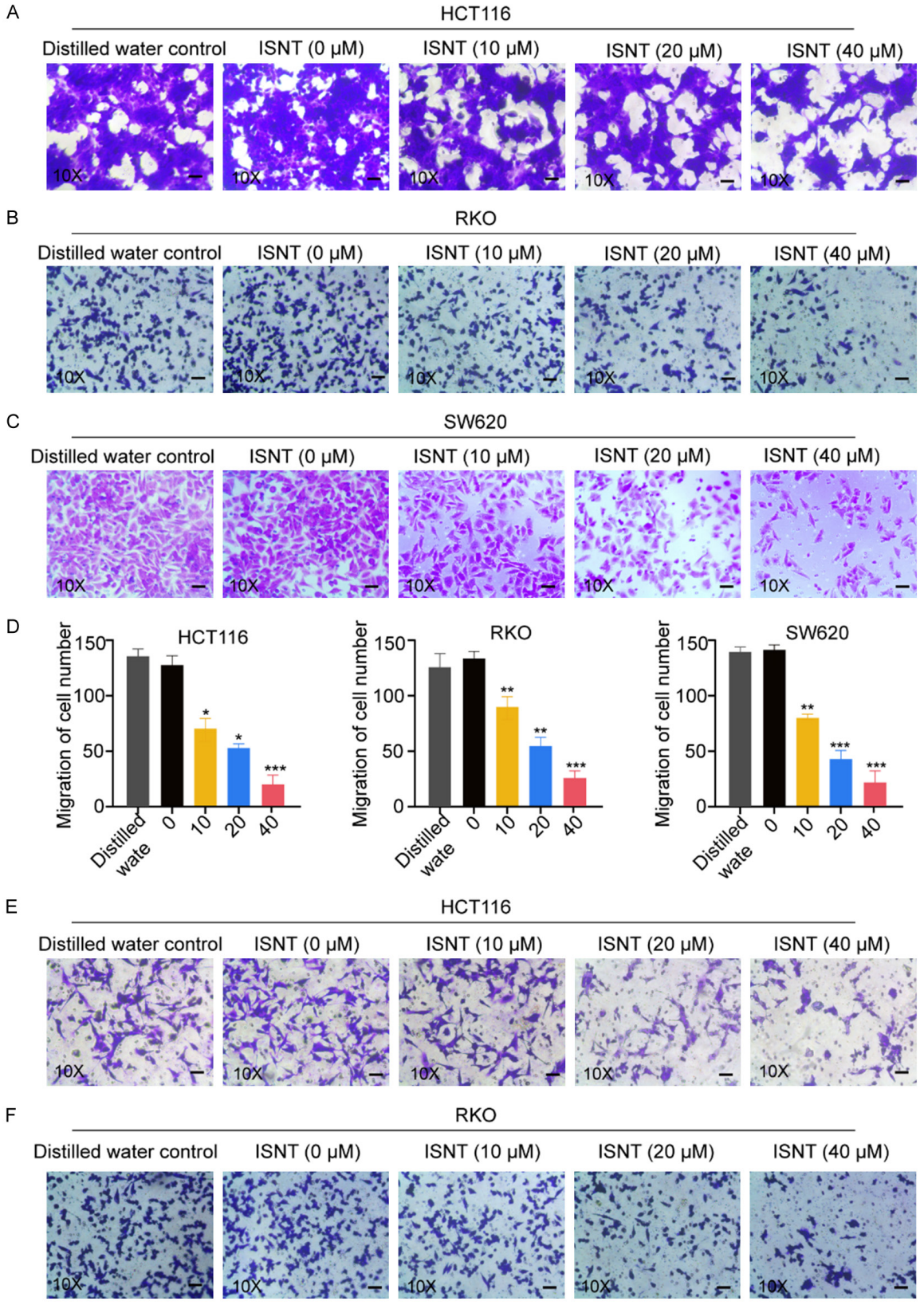

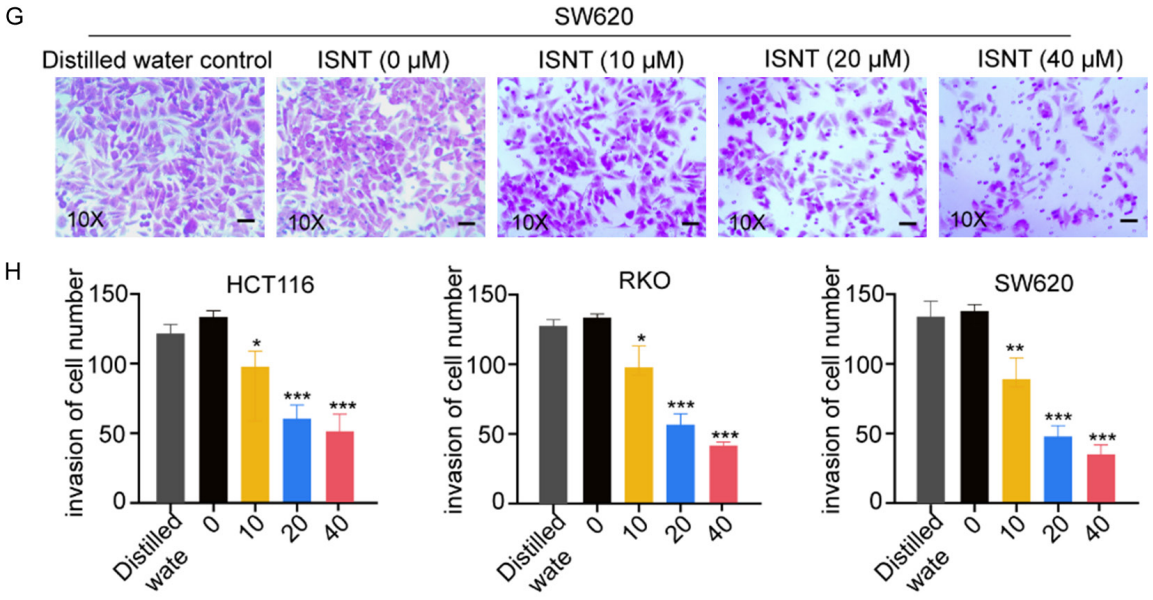

Figure 2. ISNT inhibits the migration and invasion of CRC cells in vitro. Cell migration assays for (A) HCT116, (B) RKO and (C) SW620 cells treated with different concentrations of ISNT. Scale bars represent 100 μm. (D) Statistics of the number of migrating cells in the three cell lines. Transwell assays performed on (E) HCT116, (F) RKO and (G) SW620 cells treated with various concentrations of ISNT. Scale bars represent 100 μm. (H) Statistics of the number of invasive cells in the three cell lines. Compared with the control group (ISNT of 0 μm), ***P<0.001, **P<0.01, *P<0.05.

weight remained stable across all groups (**Figure 4A**), while both tumor volume and weight were significantly reduced in ISNT-treated groups compared to controls (**Figure 4B-D**). Histological analysis via HE staining of liver and kidney tissues revealed no pathological changes in ISNT-treated mice relative to controls (**Figure 4E**), confirming the lack of hepatorenal toxicity. These data demonstrate that ISNT effectively inhibits CRC tumor growth in vivo without systemic toxicity.

ISNT downregulates USP10 and promotes c-Myc degradation

To explore the molecular mechanism, we focused on c-Myc, a key transcription factor linked to CRC cell growth, proliferation, metastasis, and stemness [23, 24]. Western blot and RT-qPCR analyses, combined with pull-down assays, revealed that ISNT reduced c-Myc protein expression in a dose-dependent manner (**Figure 5A**) without altering mRNA levels (**Figure 5B**) in HCT116 cells. Pull-down assays using a c-Myc antibody showed diminished interaction with the deubiquitinating enzyme USP10 in ISNT-treated cells, particularly at 20 μM (**Figure 5C**) [25, 26]. Western blot and RT-qPCR confirmed that ISNT downregulated USP10 expression at both protein and mRNA levels (**Figure 5D**, **5E**). Luciferase reporter assays demonstrated that ISNT significantly inhibited USP10 promoter activity (**Figure 5F**). Pre-treatment with the proteasome inhibitor MG132 abrogated ISNT-induced c-Myc degradation (**Figure 5G**), while ubiquitination assays showed that ISNT enhanced c-Myc ubiquitination (**Figure 5H**). Collectively, these findings indicate that ISNT suppresses USP10 transcription, promoting c-Myc ubiquitination and proteasomal degradation to exert its anti-CRC effects.

Discussion

Isosinensetin (ISNT), a natural polymethoxyflavone, exhibits diverse pharmacological activities across multiple disease contexts. For instance, it inhibits osteoclastogenesis by reducing reactive oxygen species, alleviating estrogen-deficiency-induced osteoporosis in mice and positioning itself as a potential therapeutic agent for osteoporosis [27]. In anti-inflammatory research, ISNT mitigates Particulate Matter 2.5 (PM2.5)-induced damage to human bronchial epithelial cells, underscoring its protective effects against environmental stressors [28]. Flavonoids, a broader class of compounds including ISNT, are well-estab-

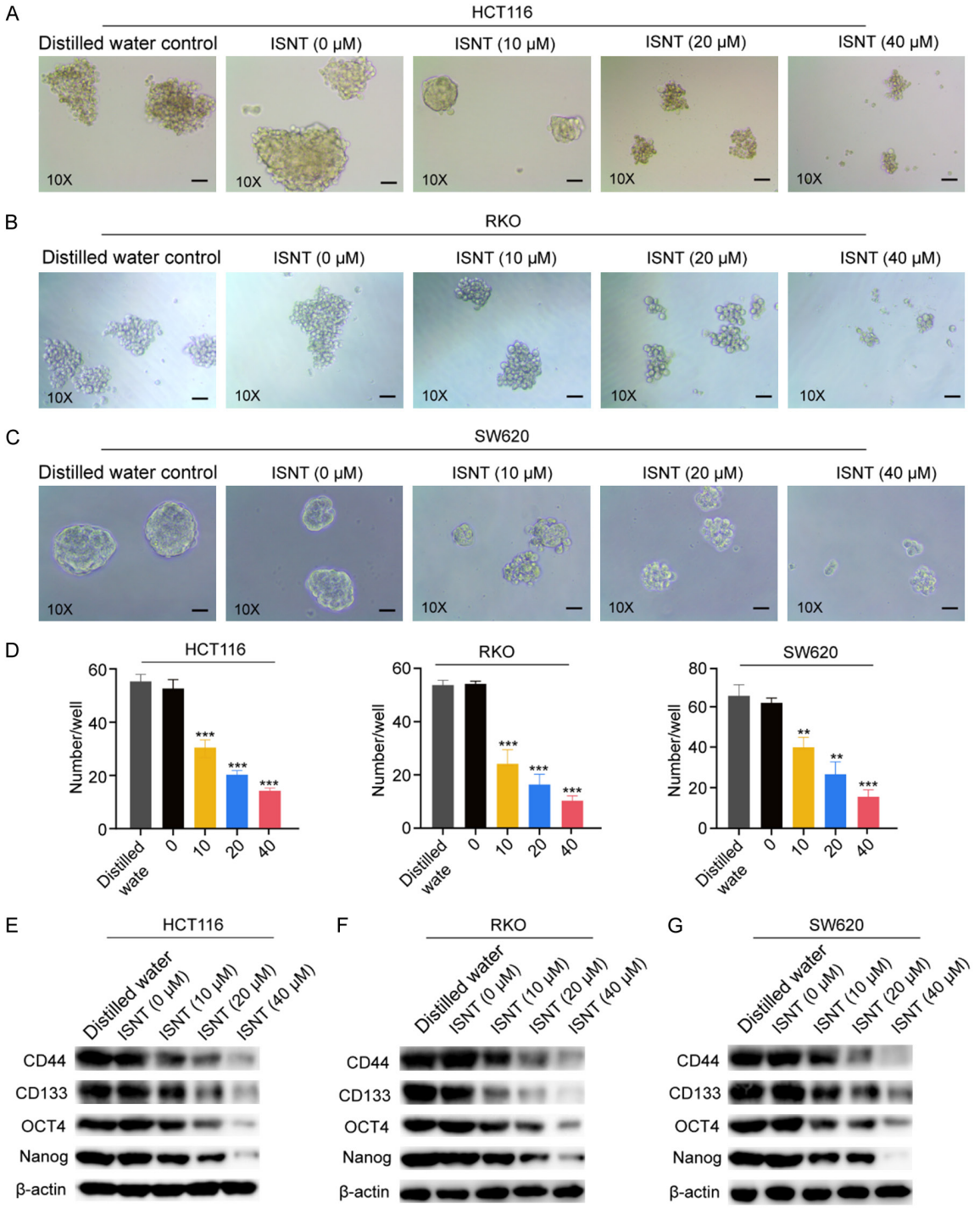

Figure 3. ISNT inhibits the stemness of CRC cells in vitro. A: Representative images of tumor spheres in HCT116 control and ISNT-treated groups. B: Representative images of tumor spheres in RKO cells treated with different concentrations of ISNT. C: Representative images of tumorsphere formation in SW620 cells exposed to distinct concentrations of ISNT. Scale bars represent 100 μm. D: Statistics on the number of tumor microspheres formed in three cell lines. E-G: Western blot analysis of protein expression of tumor stem cell markers after ISNT treatment. Compared with the control group (ISNT of 0 μm), ***P<0.001, **P<0.01.

lished for their anticancer mechanisms, such as scavenging free radicals, inhibiting tumor cell proliferation, and inducing apoptosis [13, 29]. However, despite these insights, ISNT's

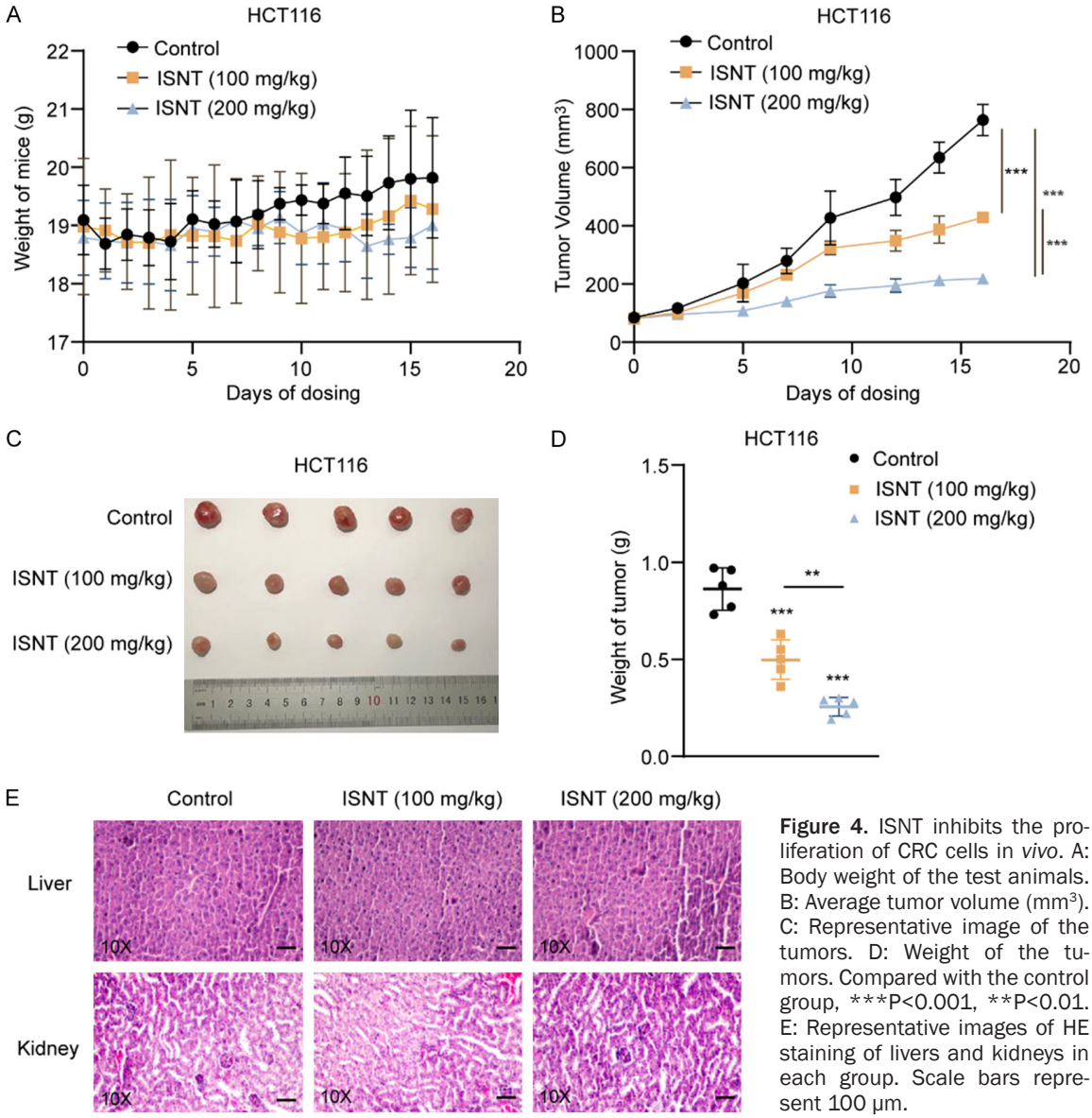

Figure 4. ISNT inhibits the proliferation of CRC cells in *vivo*. A: Body weight of the test animals. B: Average tumor volume (mm^3). C: Representative image of the tumors. D: Weight of the tumors. Compared with the control group, ***P<0.001, **P<0.01. E: Representative images of HE staining of livers and kidneys in each group. Scale bars represent 100 μm.

direct anticancer effects in colorectal cancer (CRC) have remained underexplored.

The development of CRC involves complex, multigene, multistep processes, with dysregulated signaling pathways like Notch and microRNAs (miRNAs) playing pivotal roles in tumor progression [30]. Current treatment strategies primarily rely on chemotherapy (e.g., 5-fluorouracil [5-FU] and combination regimens like FOLFOX, FOLFIRI, and CAPOX) and targeted therapies (e.g., EGFR inhibitors cetuximab/panitumumab and VEGF inhibitor bevacizumab). While chemotherapy has improved outcomes, it is limited by systemic toxicity, poor selectivity, and acquired resistance. Targeted therapies offer precision but similarly face challenges like drug resistance, highlighting the need for novel adjunctive treatments.

This study is the first to systematically investigate ISNT's anti-CRC activity using integrated in vitro and in vivo approaches. MTT assays revealed that increasing concentrations of ISNT dose-dependently reduced viability in HCT116, RKO, and SW620 cells, indicating potent inhibition of proliferation. Transwell migration and invasion assays further demonstrated that ISNT suppresses metastatic potential in these cell lines, collectively establishing its efficacy

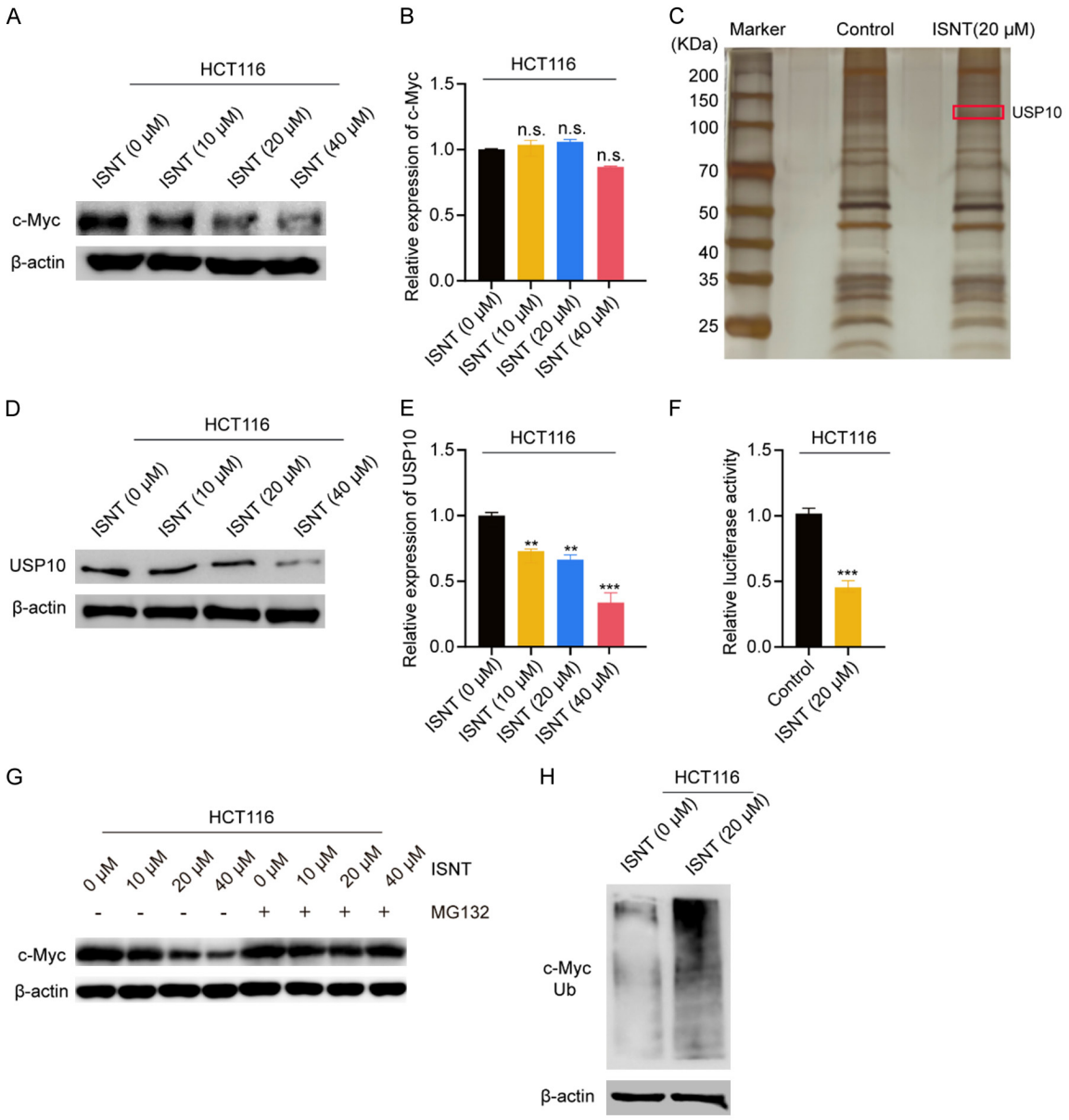

Figure 5. ISNT down-regulated USP10 and induced degrdation of c-Myc. A: WB analysis of c-Myc expression after treatment with different concentrations of ISNT. B: RT-qPCR analysis of c-Myc mRNA levels in HCT116 cells post-ISNT treatment. C: Proteomic reactivity profiles for HCT116 cell lysates in control and ISNT-treated groups. D: WB analysis of USP10 expression after treatment with different concentrations of ISNT. E: RT-qPCR analysis of USP10 mRNA levels in HCT116 cells post-ISNT treatment. F: The changes of ISNT-induced luciferase activity in the USP10 promoter in HCT116 cells. G: Treatment with MG132 (10 μM) showed that ISNT could rescue c-Myc expression. H: Western blot analysis of ubiquitin accumulation on c-Myc protein in DMSO and ISNT-treated groups. Compared with the control group (ISNT of 0 μm), ***P<0.001, **P<0.01, n.s. No statistical difference.

against key oncogenic phenotypes. In vivo, intraperitoneal injection of ISNT in tumor-bearing nude mice significantly reduced tumor volume and weight, with no observed systemic toxicity. Notably, ISNT also disrupted tumor sphere formation in a dose-dependent manner, suggesting suppression of cancer stem cell (CSC) properties.

To uncover the molecular basis of ISNT's effects, Western blotting and RT-qPCR revealed that ISNT reduces c-Myc protein expression without altering mRNA levels, implying post-translational regulation. Pull-down assays linked c-Myc destabilization to reduced interaction with the deubiquitinase USP10. Further analyses confirmed that ISNT downregulates

USP10 at both the transcriptional and translational levels, enhancing c-Myc ubiquitination and proteasomal degradation. These findings establish a novel mechanism whereby ISNT inhibits CRC progression by suppressing USP10-mediated c-Myc stabilization.

This study provides the first evidence of ISNT's anti-CRC activity, highlighting its potential as a natural product-based therapeutic. By targeting the USP10/c-Myc axis, ISNT offers a promising strategy to combat proliferation, metastasis, and stemness in CRC. However, additional research is needed to fully characterize its safety profile, optimize dosing regimens, and explore combinations with existing therapies. Future studies should also investigate whether ISNT regulates other CRC-relevant pathways (e.g., Notch, Wnt/β-catenin) and validate its efficacy in preclinical models representing diverse CRC subtypes. Collectively, these findings lay a foundation for advancing ISNT toward translational research in oncology.

Acknowledgements

This work was supported by the Basic Foundation of the Xingtai Central Hospital.

Disclosure of conflict of interest

None.

Abbreviations

CRC, colorectal cancer; LC-MS/MS, Liquid Chromatography Tandem-mass Spectrometry; PBS, phosphate-buffered saline; PMSF, phenylmethanesulfonyl fluoride; WB, Western blotting; SDS-PAGE, sodium dodecyl sulfate polyacrylamide gel electrophoresis.

Address correspondence to: Dr. Yao-Hui Yuan, Xingtai Central Hospital, No. 108 Gangtiebei Road, Xindu District, Xingtai 054000, Hebei, China. Tel: +86-15803198678; Fax: +86-319-2624466; E-mail: yyhui8678@126.com

References

[1] Sung H, Ferlay J, Siegel RL, Laversanne M, Soerjomataram I, Jemal A and Bray F. Global cancer statistics 2020: GLOBOCAN estimates of incidence and mortality worldwide for 36 cancers in 185 countries. CA Cancer J Clin 2021; 71: 209-249.

[2] Arnold M, Sierra MS, Laversanne M, Soerjomataram I, Jemal A and Bray F. Global patterns and trends in colorectal cancer incidence and mortality. Gut 2017; 66: 683-691.

[3] Miller KD, Nogueira L, Mariotto AB, Rowland JH, Yabroff KR, Alfano CM, Jemal A, Kramer JL and Siegel RL. Cancer treatment and survivorship statistics, 2019. CA Cancer J Clin 2019; 69: 363-385.

[4] Yuan J, Luo K, Zhang L, Cheville JC and Lou Z. USP10 regulates p53 localization and stability by deubiquitinating p53. Cell 2010; 140: 384-396.

[5] Deng M, Yang X, Qin B, Liu T, Zhang H, Guo W, Lee SB, Kim JJ, Yuan J, Pei H, Wang L and Lou Z. Deubiquitination and activation of AMPK by USP10. Mol Cell 2016; 61: 614-624.

[6] Liu J, Xia H, Kim M, Xu L, Li Y, Zhang L, Cai Y, Norberg HV, Zhang T, Furuya T, Jin M, Zhu Z, Wang H, Yu J, Li Y, Hao Y, Choi A, Ke H, Ma D and Yuan J. Beclin1 controls the levels of p53 by regulating the deubiquitination activity of USP10 and USP13. Cell 2011; 147: 223-234.

[7] Zhai S, Lin J, Ji Y, Zhang R, Zhang Z, Cao Y, Liu Y, Tang X, Liu J, Liu P, Lin J, Li F, Li H, Shi Y, Fu D, Deng X and Shen B. A microprotein N1DARP encoded by LINC00261 promotes Notch1 intracellular domain (N1ICD) degradation via disrupting USP10-N1ICD interaction to inhibit chemoresistance in Notch1-hyperactivated pancreatic cancer. Cell Discov 2023; 9: 95.

[8] Zeng Z, Wu HX, Zhan N, Huang YB, Wang ZS, Yang GF, Wang P and Fu GH. Prognostic significance of USP10 as a tumor-associated marker in gastric carcinoma. Tumour Biol 2014; 35: 3845-3853.

[9] Zhu H, Yan F, Yuan T, Qian M, Zhou T, Dai X, Cao J, Ying M, Dong X, He Q and Yang B. USP10 promotes proliferation of hepatocellular carcinoma by deubiquitinating and stabilizing YAP/TAZ. Cancer Res 2020; 80: 2204-2216.

[10] Lim R, Sugino T, Nolte H, Andrade J, Zimmermann B, Shi C, Doddaballapur A, Ong YT, Wilhelm K, Fasse JWD, Ernst A, Kaulich M, Husnjak K, Boettger T, Guenther S, Braun T, Krüger M, Benedito R, Dikic I and Potente M. Deubiquitinase USP10 regulates notch signaling in the endothelium. Science 2019; 364: 188-193.

[11] Atanasov AG, Zotchev SB and Dirsch VM; International Natural Product Sciences Taskforce; Supuran CT. Natural products in drug discovery: advances and opportunities. Nat Rev Drug Discov 2021; 20: 200-216.

[12] Atanasov AG, Waltenberger B, Pferschy-Wenzig EM, Linder T, Wawrosch C, Uhrin P, Temml V, Wang L, Schwaiger S, Heiss EH, Rollinger JM, Schuster D, Breuss JM, Bochkov V, Mihovilovic MD, Kopp B, Bauer R, Dirsch VM and Stuppner

H. Discovery and resupply of pharmacologically active plant-derived natural products: a review. Biotechnol Adv 2015; 33: 1582-1614.
[13] Kim H, Moon JY, Mosaddik A and Cho SK. Induction of apoptosis in human cervical carcinoma HeLa cells by polymethoxylated flavone-rich Citrus grandis Osbeck (Dangyuja) leaf extract. Food Chem Toxicol 2010; 48: 2435-2442.
[14] Sood S, Arora B, Bansal S, Muthuraman A, Gill NS, Arora R, Bali M and Sharma PD. Antioxidant, anti-inflammatory and analgesic potential of the Citrus decumana L. peel extract. Inflammopharmacology 2009; 17: 267-274.
[15] Miyazawa M, Okuno Y, Fukuyama M, Nakamura S and Kosaka H. Antimutagenic activity of polymethoxyflavonoids from Citrus aurantium. J Agric Food Chem 1999; 47: 5239-5244.
[16] Balestrieri E, Pizzimenti F, Ferlazzo A, Giofrè SV, Iannazzo D, Piperno A, Romeo R, Chiacchio MA, Mastino A and Macchi B. Antiviral activity of seed extract from Citrus bergamia towards human retroviruses. Bioorg Med Chem 2011; 19: 2084-2089.
[17] Soudani N, Rafrafi M, Ben Amara I, Hakim A, Troudi A, Zeghal KM, Ben Salah H, Boudawara T and Zeghal N. Oxidative stress-related lung dysfunction by chromium(VI): alleviation by Citrus aurantium L. J Physiol Biochem 2013; 69: 239-253.
[18] Kurowska EM and Manthey JA. Hypolipidemic effects and absorption of citrus polymethoxylated flavones in hamsters with diet-induced hypercholesterolemia. J Agric Food Chem 2004; 52: 2879-2886.
[19] Shao D, Liu X, Wu J, Zhang A, Bai Y, Zhao P and Li J. Identification of the active compounds and functional mechanisms of Jinshui Huanxian formula in pulmonary fibrosis by integrating serum pharmacochemistry with network pharmacology. Phytomedicine 2022; 102: 154177.
[20] Lee SH, Ko HM, Jee W, Kim H, Chung WS and Jang HJ. Isosinensetin stimulates glucagon-like peptide-1 secretion via activation of hTAS2R50 and the G (βγ)-mediated signaling pathway. Int J Mol Sci 2023; 24: 3682.
[21] Zheng H, Liu H, Li H, Dou W, Wang J, Zhang J, Liu T, Wu Y, Liu Y and Wang X. Characterization of stem cell landscape and identification of stemness-relevant prognostic gene signature to aid immunotherapy in colorectal cancer. Stem Cell Res Ther 2022; 13: 244.
[22] Ricci-Vitiani L, Lombardi DG, Pilozzi E, Biffoni M, Todaro M, Peschle C and De Maria R. Identification and expansion of human colon-cancer-initiating cells. Nature 2007; 445: 111-115.
[23] Dalla-Favera R, Bregni M, Erikson J, Patterson D, Gallo RC and Croce CM. Human c-myc onc gene is located on the region of chromosome 8 that is translocated in Burkitt lymphoma cells. Proc Natl Acad Sci U S A 1982; 79: 7824-7827.
[24] Dang CV. MYC on the path to cancer. Cell 2012; 149: 22-35.
[25] Lin Z, Yang H, Tan C, Li J, Liu Z, Quan Q, Kong S, Ye J, Gao B and Fang D. USP10 antagonizes c-Myc transcriptional activation through SIRT6 stabilization to suppress tumor formation. Cell Rep 2013; 5: 1639-1649.
[26] Wang C, Ni J, Zhai D, Xu Y, Wu Z, Chen Y, Liu N, Du J, Shen Y, Liu G, Yang Y, You L and Hu W. Stress-induced epinephrine promotes hepatocellular carcinoma progression via the USP10-PLAGL2 signaling loop. Exp Mol Med 2024; 56: 1150-1163.
[27] Qin Y, Song D, Liao S, Chen J, Xu M, Su Y, Lian H, Peng H, Wei L, Chen K, Xu J, Zhao J and Liu Q. Isosinensetin alleviates estrogen deficiency-induced osteoporosis via suppressing ROS-mediated NF-κB/MAPK signaling pathways. Biomed Pharmacother 2023; 160: 114347.
[28] Zou Y, Li S, Li X, Sun Y, Ma M, Tian H, Wang N, Yuan J and Xiao C. Isosinensetin alleviates the injury of human bronchial epithelial cells induced by PM (2.5). Exp Ther Med 2021; 22: 1435.
[29] Bai J, Zhao S, Fan X, Chen Y, Zou X, Hu M, Wang B, Jin J, Wang X, Hu J, Zhang D and Li Y. Inhibitory effects of flavonoids on P-glycoprotein in vitro and in vivo: food/herb-drug interactions and structure-activity relationships. Toxicol Appl Pharmacol 2019; 369: 49-59.
[30] Borzacchiello L, Veglia Tranchese R, Grillo R, Arpino R, Mosca L, Cacciapuoti G and Porcelli M. S-adenosylmethionine inhibits colorectal cancer cell migration through mirna-mediated targeting of notch signaling pathway. Int J Mol Sci 2022; 23: 7673.